Snap-back repellers and chaos in a class of discrete-time memristor circuits

Mauro Di Marco · Mauro Forti · Luca Pancioni · Alberto Tesi

Abstract In the last decade the flux-charge analysis method (FCAM) has been successfully used to show that continuous-time (CT) memristor circuits possess for structural reasons first integrals (invariants of motion) and their state space can be foliated in invariant manifolds. Consequently, they display an initial condition dependent dynamics, extreme multistability (coexistence of infinitely many attractors) and bifurcations without parameters. Recently, a new discretization scheme has been introduced for CT memristor circuits, guaranteeing that the first integrals are preserved exactly in the discretization. On this basis, FCAM has been extended to discrete-time (DT) memristor circuits showing that they also are characterized by invariant manifolds and they display extreme multistability and bifurcations without parameters. This manuscript considers the maps obtained via DT-FCAM for a circuit with a flux-controlled memristor and a capacitor and it provides a thorough and rigorous investigation of the presence of chaotic dynamics. In particular, parameter ranges are obtained where the maps have snap-back repellers at some fixed points, thus implying that they display chaos in the Marotto and also in the Li–Yorke sense. Bifurcation diagrams are provided where it is possible to analytically identify relevant points in correspondence with the appearance of snap-back repellers and the onset of chaos. The dependence of the bifurcation diagrams and snap-back repellers upon the circuit initial conditions and the related manifold is also studied.

M. Di Marco · M. Forti (✉) · L. Pancioni
Department of Information Engineering and Mathematics,
University of Siena, via Roma 56, 53100 Siena, Italy
e-mail: mauro.forti@unisi.it

M. Di Marco
e-mail: mauro.dimarco@unisi.it

L. Pancioni
e-mail: luca.pancioni@unisi.it

A. Tesi
Department of Information Engineering, University of Florence,
via S. Marta 3, 50139 Florence, Italy
e-mail: alberto.tesi@unifi.it

1 Introduction

Memristors are passive electronic elements enjoying the two main features of *nonlinearity* and *memory* [1,2]. It is well known that memristors can greatly enrich the dynamic behaviors of continuous-time (CT) analog circuits with respect to the traditional nonlinear RLC circuits [3–11]. Among many applications, memristor circuits can be effectively used as sources of complex dynamic behaviors for real-time signal processing and the solution of combinatorial optimization problems [12–14]. Due to their memory, memristors also

make it possible to implement in-memory computing schemes where the processing and the memorization of the results are performed by the same devices, as it happens for biological neurons. In principle this permits to overcome drawbacks of Von Neumann machines where the information needs to be continuously moved between the central processing unit (CPU) and memory (e.g., the RAM), that are located at different physical sites [15–18]. The rich dynamics typically displayed and the possibility of exploiting in-memory computing make the use of memristors an enabling technology that is expected to play an increasingly relevant role in future electronics systems and neuromorphic brain-like computers.

Recently, discrete-time (DT) memristor circuits have received an ever increasing attention. The first motivation is that discretized versions of memristor circuits can be directly implemented in software on digital computers or other types of digital signal processors, such as a reconfigurable hardware emulator on a field programmable gate array (FPGA) or an application specific integrated circuit (ASIC) [11,19]. Moreover, since the availability of analog memristor devices is still limited, digital memristor emulators play a relevant role to assess the performances of actual memristor circuits [20,21]. Most importantly, in addition to emulate the dynamics of CT memristor circuits, maps implemented by DT memristor circuits are of interest in themselves as a *source of complex dynamics for engineering applications* in the field of random number generation [22], secure communications [23], reservoir computing [24] and biomedical image encryption [25,26].

Broadly speaking, the literature on the dynamics of DT memristor circuits can be subdivided into two main topics:

1. Chaos and hyperchaos generated by maps of DT memristor circuits and techniques to enhance the complexities of hyperchaotic memristor maps ([23, 27–33] and references therein).
2. Coexistence of different chaotic attractors, initial condition dependent dynamic behaviors, multistability and extreme multistability for special types of memristor maps ([29,34–36] and references therein).

Although there are already relevant contributions, one limitation is that several dynamical results are obtained by using numerical means and simulations. For instance, chaos and hyperchaos are studied mainly by computing numerically bifurcation diagrams and Lyapunov exponents of the DT maps, while multistability and extreme multistability are studied by using sets of simulations with different initial conditions. However, it would be desirable to delve deeper into these topics and give a more solid foundation to complex dynamics and extreme multistability of these maps by means of analytic techniques.

In [2,37,38], a technique has been devised, named flux-charge analysis method (FCAM), showing that CT circuits with ideal memristors possess for structural reasons *first integrals* (or invariants of motion). As a consequence, their state space can be foliated in invariant manifolds where a different, initial condition dependent dynamics, is displayed. This gives an analytic explanation of the presence of infinitely many coexisting attractors, also known as *extreme multistability*, and the bifurcations without parameters that can be observed in CT memristor circuits. Very recently, a *new discretization scheme* has been introduced for the memristor guaranteeing that the *first integrals of CT memristor circuits are preserved exactly in the discretization*. In particular, the paper [39] extended FCAM to DT memristor circuits showing also for such circuits the existence of invariant manifolds in the state space and the peculiar phenomena of extreme multistability and bifurcations without parameters.

The main goal of this manuscript is to use *rigorous definitions of chaos* and employ *analytic methods to prove chaos* in some memristor maps obtained via the new discretization scheme introduced in [39]. The first definition of chaos in a scalar difference equation has been given by Li and Yorke in 1975 [40]. Three years later, Marotto proposed a generalization to multidimensional difference equations [41]. Marotto's technique is based on the concept of a snap-back repeller at a fixed point as well as on the fundamental property stating that the existence of a snap-back repeller implies chaos in the Marotto and also in the Li–Yorke sense. Here, we consider the maps obtained in [39] for a DT circuit with a capacitor and a flux-controlled memristor. The maps are second-order in the standard voltage-current domain while they are first-order on each invariant manifold in the flux-charge domain. The main contribution of this paper is a deep analytic investigation of chaos for the considered DT memristor circuits. Especially, analytic results are established on the existence of snap-back repellers for the first-order map on each invariant manifold, thus rigorously proving chaos in the

Marotto and Li–Yorke sense. Bifurcations diagrams are studied in detail and the dependence of these diagrams and snap-back repellers upon the invariant manifold and initial conditions is also addressed.

The structure of the paper is outlined as follows. Some preliminary results about maps and chaos in the Marotto sense are given at the end of this section. Then, Sect. 2 briefly reviews the new memristor discretization scheme proposed in [39] and introduces the maps generated by the considered class of DT memristor circuits. Sections 3 and 4 contain the main results in the manuscript on snap-back repellers and Marotto chaos for the considered maps. Finally, Sect. 5 discusses the obtained results while Sect. 6 collects some main concluding remarks.

1.1 Preliminaries

1.1.1 Difference equations

Consider the difference equation (or map)

$$x_{k+1} = f(x_k), \quad k = 0, 1, 2, \dots$$

where $x_k \in \mathbb{R}^n$, $f : \mathbb{R}^n \to \mathbb{R}^n$ and $f \in C^1(\mathbb{R}^n)$. The iterates of a point x_0 under f are defined as $x_0 = f^0(x_0)$, $x_1 = f^1(x_0) = f(x_0)$, $x_k = f^k(x_0) = f(f^{k-1}(x_0))$, $k = 2, 3, \dots$, i.e., f^k is the k-fold composition of f with itself.

For any $y \in \mathbb{R}^n$ we let $F^{-1}(y) = \{x \in \mathbb{R}^n : f(x) = y\}$. We may have $F^{-1}(y) = \emptyset$. When f is not injective, it may also happen that $F^{-1}(y)$ is multi-valued, i.e., it has more than one element. Each point in $F^{-1}(y)$ is said to be a backward iterate (or pre-image) of y through f. In a similar way we can define $F^{-k}(y)$ for $k \geq 2$.

A periodic point of period q of f is a point x_p which maps back to itself under q iterates of the map, i.e., $f^q(x_p) = x_p$ and $f^k(x_p) \neq x_p$ for any $0 < k < q$. The collection $\{f^k(x_p)\}_{k=1}^q$ is said to be a q-cycle. When $q = 1$ a periodic point $\bar{x}$ is said to be a fixed point of the map and it satisfies $f(\bar{x}) = \bar{x}$.

A set $Q \subset \mathbb{R}^p$ is positively invariant if $f(Q) \subset Q$. In this case, for any $x_0 \in Q$, we have $f^k(x_0) \in Q$, $k = 1, 2, \dots$. If we have $f(Q) = Q$, then Q is invariant and any pre-image of $y \in Q$ also belongs to Q.

1.1.2 Snap-back repellers

The definition of a *snap-back repeller* according to Marotto is given in [41]. After publication of that paper, it was found that the original definition of a snap-back repeller was not adequate to prove chaos. In [42], this problem has been solved by introducing a slightly different definition that is given below.

Definition 1 A fixed point $z \in \mathbb{R}^n$ of the map f is said to be a *snap-back repeller* if:

(i) there exists $r > 0$ such that all eigenvalues of $(Df(x))^{\top} Df(x)$ are greater than 1 when $x \in B_r(z) = \{x \in \mathbb{R}^n : \|x - z\| \leq r\}$, where $\|\cdot\|$ is the Euclidean-norm and $Df(\cdot)$ is the Jacobian of f;

(ii) there exist a point $z_0 \in B_r(z)$, $z_0 \neq z$, and a positive integer m such that $f^m(z_0) = z$ and the determinant $\det(Df^m(z_0)) \neq 0$.

If there is a snap-back repeller of the map, then the map is chaotic in the sense of Marotto, according to the next definition.

Definition 2 [41] The map f is chaotic in the sense of Marotto if:

(a) There exists a positive integer N such that, for each integer $q \geq N$, f has a periodic point of period q;

(b) there exists a *scrambled set* of f, namely, an uncountable set S containing no periodic points of f such that:

(b1) $f(S) \subset S$;

(b2) for any $x, y \in S$, $x \neq y$, we have

$$\limsup_{k \to \infty} \|f^k(x) - f^k(y)\| > 0;$$

(b3) for any $x \in S$ and any periodic point x_p of f we have

$$\limsup_{k \to \infty} \|f^k(x) - f^k(x_p)\| > 0;$$

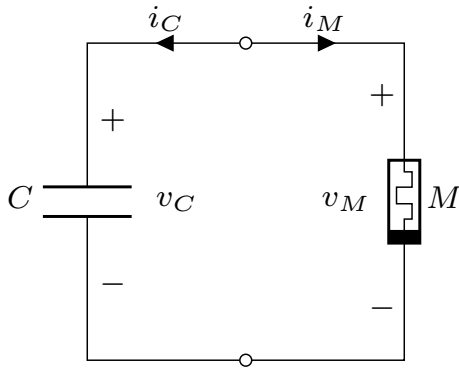(b4) there exists an uncountable subset S_0 of S such that for any $x, y \in S_0$ we have

Fig. 1 Continuous-time memristor-capacitor circuit (CT-MCC)

$$\lim_{k \to \infty} \inf \| f^k(x) - f^k(y) \| = 0.$$

It is known that if f is chaotic in the sense of Marotto, then it is also chaotic in the sense of Li–Yorke [42].

Finally, we remark that for a scalar map, i.e., $n = 1$, the definition of a snap-back repeller simplifies as follows.

Definition 3 Let $n = 1$. A fixed point $z \in \mathbb{R}$ of the map f is said to be a *snap-back repeller* if:

(i) there exists $r > 0$ such that $|f'(x)| > 1$ when $x \in B_r(z) = \{x \in \mathbb{R} : |x - z| \le r\}$;
(ii) there exist a point $z_0 \in B_r(z)$, $z_0 \ne z$, and a positive integer m such that $f^m(z_0) = z$ and $(f^m)'(z_0) \ne 0$.

2 Discrete-time memristor-capacitor circuit

Consider the continuous-time (CT) memristor-capacitor circuit (MCC) in Fig. 1 with an ideal capacitor C and an ideal flux-controlled memristor M. We wish to study a DT version of the circuit, named DT-MCC, via the DT-FCAM introduced in [39]. That method is based on using a special discretization scheme for the memristor that preserves exactly the first integrals of the CT-MCC, and then analyzing the obtained DT circuit both in the voltage-current domain (VCD) and flux-charge domain (FCD). Next, we briefly recall some basic facts about DT-FCAM and apply the method to obtain the maps describing the dynamics of the DT-MCC.

Let v (resp., i) be the voltage (resp., current) of a two-terminal electric element. Define the flux $\varphi(t) = \int_{-\infty}^{t} v(t)dt$ and charge $q(t) = \int_{-\infty}^{t} i(t)dt$. For $t \ge 0$, also define the incremental flux $\varphi^0(t) = \varphi(t) - \varphi(0) = \int_0^t v(t)dt$ and incremental charge $q^0(t) = q(t) - q(0) = \int_0^t i(t)dt$ [37]. Given the sampling instants $t_k = kh$, $k = 0, 1, 2, \ldots$, where $h > 0$ is the step size, the corresponding discrete electric quantities are $v_k = v(t_k)$, $i_k = i(t_k)$, $\varphi_k = \varphi(t_k)$, $q_k = q(t_k)$, $\varphi_k^0 = \varphi^0(t_k)$ and $q_k^0 = q^0(t_k)$.

Let C be a linear capacitor satisfying $q_C = Cv_C$, or, $i_C = C\dot{v}_C$. By applying forward Euler rule we obtain in the VCD the first-order map

$$i_{C,k} = C \frac{v_{C,k+1} - v_{C,k}}{h}. \tag{1}$$

In the FCD, in terms of incremental flux and charge, C obeys the first-order map

$$q_{C,k}^0 = C \frac{\varphi_{C,k+1}^0 - \varphi_{C,k}^0}{h} - Cv_{C,0} \tag{2}$$

where $v_{C,0} = v_C(0)$.

Consider now a flux-controlled memristor M satisfying $q_M = \hat{q}(\varphi_M)$. By differentiating in time, we have

$$\begin{cases} i_M = \dot{q}_M = \hat{q}'(\varphi_M)v_M \\ \dot{\varphi}_M = v_M. \end{cases} \tag{3}$$

The quantity $\hat{q}'(\varphi_M)$ has dimension of Ohm^{-1} and is named memductance. Note that a memristor satisfies a state-dependent Ohm's law where the the memductance is not a constant as in a traditional resistor, but rather is a function of the memristor state $\varphi_M(t) = \int_{-\infty}^{t} v_M(\sigma)d\sigma$ and hence it takes into account the full history of the voltage applied to the memristor [2].

In [39], a new discretization scheme of (3) has been introduced in the VCD as follows. By applying forward Euler rule to $i_M = \dot{q}_M$ we have $i_{M,k} = (q_{M,k+1} - q_{M,k})/h = (\hat{q}(\varphi_{M,k+1}) - \hat{q}(\varphi_{M,k}))/h$. This yields

$$\begin{cases} i_{M,k} = \frac{1}{h}(\hat{q}(\varphi_{M,k+1}) - \hat{q}(\varphi_{M,k})) \\ \varphi_{M,k+1} = \varphi_{M,k} + hv_{M,k}. \end{cases} \tag{4}$$
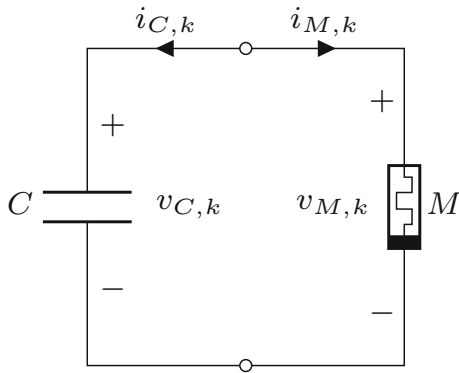
Fig. 2 Discrete-time memristor-capacitor circuit (DT-MCC)

In the FCD we simply obtain the first-order algebraic map

$$q_{M,k}^0 = \hat{q}(\varphi_{M,k}^0 + \varphi_{M,0}) - \hat{q}(\varphi_{M,0}) \qquad (5)$$

where $\varphi_{M,0} = \varphi_M(0)$.

2.1 Analysis in the VCD

Consider the DT-MCC circuit of Fig. 2 in the VCD. Current and voltage Kirchhoff laws yield $i_{C,k} + i_{M,k} = 0$ and $v_{C,k} = v_{M,k}$, respectively. Using (1) and the discretization scheme for M given in (4), we obtain

$$C\frac{v_{C,k+1} - v_{C,k}}{h} + \frac{\hat{q}(\varphi_{M,k+1}) - \hat{q}(\varphi_{M,k})}{h} = 0.$$

Therefore, DT-MCC obeys in the VCD the second-order map

$$\begin{cases} v_{C,k+1} = v_{C,k} + \frac{1}{C}(-\hat{q}(\varphi_{M,k} + hv_{C,k}) + \hat{q}(\varphi_{M,k})) \\ \varphi_{M,k+1} = \varphi_{M,k} + hv_{C,k} \end{cases}$$
$$(6)$$

in the state variables $v_{C,k}$, $\varphi_{M,k}$. The initial conditions for the state variables in the VCD are $v_{C,0}$ and $\varphi_{M,0}$.

It is easy to see that (6) admits *integrals of motion*. Define the function of the state variables

$$w(v_C, \varphi_M) = Cv_C + \hat{q}(\varphi_M).$$

Considering that $\varphi_{M,k+1} = \varphi_{M,k} + hv_{C,k}$ and rearranging terms of the first equation in (4), we obtain

$$Cv_{C,k+1} + \hat{q}(\varphi_{M,k+1}) = Cv_{C,k} + \hat{q}(\varphi_{M,k}).$$

This means that $w(v_{C,k+1}, \varphi_{M,k+1}) = w(v_{C,k}, \varphi_{M,k})$, i.e., *$w$ is a first integral for the DT-MCC circuit and this is true for any choice of the step size h*. Moreover, the first integral coincides with that of the CT-MCC circuit [37].

Consider the subsets of the state space

$$\mathcal{M}(Q_0) = \Big\{ (v_C, \varphi_M) \in \mathbb{R}^2 :$$
$$w(v_C, \varphi_M) = Cv_C + \hat{q}(\varphi_M); \quad w(v_C(t_0),$$
$$\varphi_M(t_0)) = Cv_{C,0} + \hat{q}(\varphi_{M,0}) \doteq Q_0 \Big\} \quad (7)$$

where t_0 is the initial instant. Each subset is a one-dimensional *invariant manifold* for the dynamics of (6) and it is uniquely defined by the *manifold index Q_0* that depends upon the initial conditions for the state variables in the VCD. Actually, any iterate of (6) starting in $\mathcal{M}(Q_0)$ is constrained to evolve in $\mathcal{M}(Q_0)$ for any $k > 0$.

Remark 1 It is of importance to stress that the new discretization scheme (4) differs from the typical scheme adopted in the literature and given by [23,28,29,33]

$$\begin{cases} i_{M,k} = \hat{q}'(\varphi_{M,k})v_{M,k} \\ \varphi_{M,k+1} = \varphi_{M,k} + hv_{M,k}. \end{cases} \qquad (8)$$

It can be easily checked that if the scheme (8) is adopted, then the obtained DT-MCC circuit no longer possesses a first integral, no matter how small the step size h is. See [39] for more details.

2.2 Analysis in the FCD

Due to the existence of a first integral, the dynamics of (6) on each invariant manifold is expected to be of lower order, i.e., first order. Next, according to DT-FCAM, we analyze the DT-MCC circuit of Fig. 3 in the FCD to determine the dynamics on an invariant manifold. From Kirchhoff charge and flux laws [39] we have $q_{C,k}^0 + q_{M,k}^0 = 0$ and $\varphi_{C,k}^0 = \varphi_{M,k}^0$, respectively. Using (2) and (5), we obtain the first-order map in the state variable $\varphi_{C,k}^0$

$$\varphi_{C,k+1}^0 = \varphi_{C,k}^0 - \frac{h}{C}\hat{q}(\varphi_{C,k}^0 + \varphi_{M,0}) + \frac{h}{C}Q_0 \qquad (9)$$

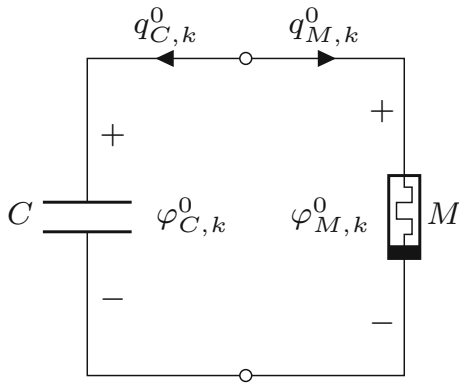where Q_0 is the manifold index given in (7).

Fig. 3 DT-MCC in the FCD

This shows that there are ∞^1 different first-order maps, in one-to-one correspondence with the manifolds $\mathcal{M}(Q_0)$. It is worth to note that each map differs from the others due to the additive term hQ_0 depending on the manifold index Q_0, i.e., on the initial conditions for the state variables in the VCD.

2.3 First-order maps in the FCD

Assume henceforth that the memristor M has the cubic nonlinearity

$$q_M = \hat{q}(\varphi_M) = -a\varphi_M + b\varphi_M^3$$

where $a, b > 0$. Since $\hat{q}$ is not monotone increasing, M is a locally active flux-controlled memristor [2]. The map (9) can be rewritten as $x_{k+1} = (1+ha)x_k - hbx_k^3 + hQ_0$, or

$$x \rightarrow f(x) = (1 + ha)x - hbx^3 + hQ_0. \qquad (10)$$

To simplify the analysis and exposition, we will consider henceforth, unless stated otherwise, the typical values $a = b = 1$. By further assuming $C = 1$ and letting $x(t) = \varphi_M(t)$, we obtain the map

$$x \rightarrow f(x) = (1 + h)x - hx^3 + hQ_0. \qquad (11)$$

This map depends upon two parameters, i.e., the step size h and the manifold index Q_0. Therefore, for the map we can envisage two conceptually different types of bifurcations, namely, bifurcations due to varying the step size h for a fixed Q_0 (i.e., a fixed manifold) and

bifurcations due to varying the initial conditions in the VCD, and hence Q_0, for fixed h and circuit parameters, the latter bifurcations being named bifurcations without parameters [2].

Next, we first study the dynamics of map (11) on manifold $\mathcal{M}(0)$, and then on manifolds $\mathcal{M}(Q_0)$ with $Q_0 \neq 0$, when parameter h is varied. Moreover, we study the dynamics for fixed h when parameter Q_0 is varied. The main goal is to find in any case parameter ranges where the existence of snap-back repellers at some fixed point of the map can be proved.

3 Snap-back repellers when $Q_0 = 0$

Consider first the case $Q_0 = 0$. Then, the map (11) on manifold $\mathcal{M}(Q_0 = 0)$ simplifies to

$$x \rightarrow f(x) = (1 + h)x - hx^3 \qquad (12)$$

and it depends upon a single parameter $h > 0$ (the step size). Figure 4 shows f for different values of h. Let $M(h)$ (resp., $-M(h)$) be the maximum (resp., minimum) of f in $[0, +\infty)$ (resp., $(-\infty, 0]$). We have

$$M(h) = \frac{2}{3} \frac{(1 + h)^{3/2}}{(3h)^{1/2}}. \qquad (13)$$

First of all, let us find for any $h > 0$ an invariant interval for the map (12) where an interesting dynamics occurs. To this end, we resort to the following geometric procedure. Consider the second iterate f^2 and solve $f^2(x) = x$, i.e., look for 2-periodic points of the map. Consider the largest solution $\alpha(h)$ of $f^2(x) = x$, i.e., the largest 2-periodic point.

Proposition 1 *The following hold.*

(i) For any $h > 0$ we have $\alpha(h) > 1$, moreover, $(f^2)'(\alpha(h)) > 1$, i.e., the 2-cycle $\alpha(h) \rightarrow -\alpha(h) \rightarrow \alpha(h)$ is unstable.

(ii) If

$$\alpha(h) \geq M(h) \qquad (14)$$

then

$$I_h \doteq [-\alpha(h), \alpha(h)]$$

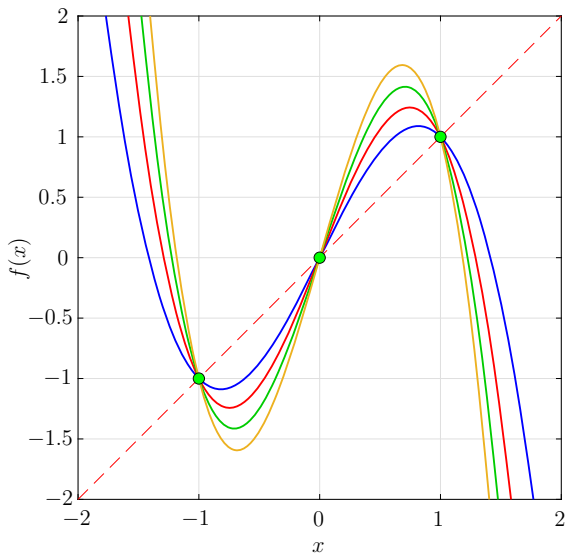**Fig. 4** Behavior of f when $h = 1$ (blue), $h = 1.5$ (red), $h = 2$ (green) and $h = 2.5$ (orange). For any h there are three fixed points $-1, 0, 1$ marked with green points. (Color figure online)

is an invariant interval for the map (12), i.e., $f(I_h) = I_h$.

Proof (i) Consider Fig. 5 showing f and f^2. We have $f^2(1) = 1$ and $f^2(\sqrt{1 + 1/h}) = f(\sqrt{1 + 1/h}) = 0$. Moreover, for x large, f^2 increases monotonically up to $+\infty$ with a slope $(f^2)'(x)$ that also tends to $+\infty$ as $x \to +\infty$. It follows that f^2 intersects $y = x$ at a point $\alpha(h) > 1$. Let us now show that $(f^2)'(\alpha(h)) > 1$. Function f^2 vanishes not only at $\sqrt{1 + 1/h}$ but also at point $\tilde{x} > \sqrt{1 + 1/h}$ such that $f(\tilde{x}) = -\sqrt{1 + 1/h}$. Considering that $f(x)$ is cubic and odd, we have that $|f'(x)|$ is increasing for any $|x| > ((1 + h)/(3h))^{1/2}$ and, similarly, $|(f^2)'(x)|$ is increasing for any $|x| > \hat{x}$ such that $|f(\hat{x})| = ((1 + h)/(3h))^{1/2}$. Taking into account that

$$0 < \sqrt{\frac{1 + h}{3h}} < \sqrt{1 + 1/h} < \hat{x} < \tilde{x} < \alpha(h)$$

to prove that $(f^2)'(\alpha(h)) > 1$ it suffices to prove that $(f^2)'(\tilde{x}) > 1$. We have $(f^2)'(\tilde{x}) = f'(f(\tilde{x}))f'(\tilde{x}) = f'(-\sqrt{1 + 1/h})f'(\tilde{x}) \geq (f'(\sqrt{1 + 1/h}))^2$ and consequently $f'(-\sqrt{1 + 1/h}) = -2(h+1)$. Since $h > 0$, $f'(-\sqrt{1 + 1/h}) \leq -2$, thus $(f^2)'(\tilde{x}) \geq 4 > 1$. This completes the proof.

(ii) Let us consider as in Fig. 5 a typical situation with a 2-cycle $\alpha(h) \to -\alpha(h) \to \alpha(h)$ and $\alpha(h) \geq M(h)$.
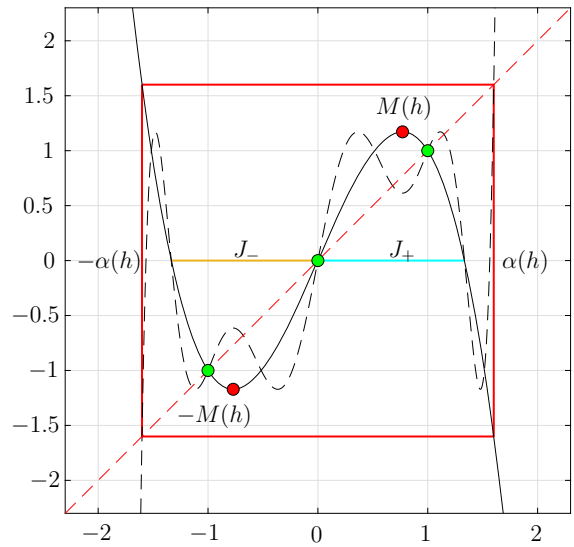

Fig. 5 Behavior of f (solid, black) and f^2 (dashed, black) when $h = 1.28$. It is seen that $f^2(x) = x$ has a solution $\alpha(h) = 1.601 > 1$. The interval $I_h = [-\alpha(h), \alpha(h)]$ is invariant, i.e., $f(I_h) = I_h$. Note the unstable 2-cycle $\alpha(h) \to -\alpha(h) \to \alpha(h)$ (red) and the intervals $J_+ = [0, \sqrt{1 + 1/h}]$ such that $f(\sqrt{1 + 1/h}) = 0$ (cyan) and $J_- = [-\sqrt{1 + 1/h}, 0]$ such that $f(-\sqrt{1 + 1/h}) = 0$ (orange). (Color figure online)
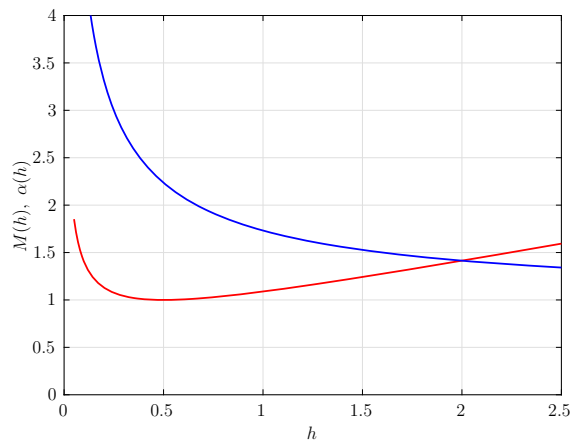

Fig. 6 Behavior of $M(h)$ (red) and $\alpha(h)$ (blue) as a function of h. We have $\alpha(h) \geq M(h)$ provided $0 < h \leq 2$. (Color figure online)

Clearly, we have $f(I_h) = I_h$ and so the interval I_h is invariant for (12). $\qquad\square$

Figure 6 shows the behavior of $\alpha(h)$ and $M(h)$ as a function of h. It is seen that $\alpha(h) \geq M(h)$ for any $0 < h \leq 2$. This is the range of h guaranteeing that $I_h = [-\alpha(h), \alpha(h)]$ is an invariant interval for f. Due to Proposition 1 and its proof, for any $0 < h \leq 2$,

iterates of (12) starting in I_h stay in I_h and are bounded. Instead, those starting outside I_h may be unbounded. Actually, $\alpha(h)$ is the largest 2-periodic point and the corresponding 2-cycle is unstable, i.e., bounded and unbounded iterates are delimited by the largest unstable cycle. If $\alpha(h) < M(h)$, then $f(I_h) \not\subset I_h$ and iterates starting in I_h may exit I_h and grow unboundedly.

Consider now the map $f : I_h \to I_h$ for $0 < h \le 2$. Solving $f(x) = x$ we obtain that for any h there are three fixed points $0, 1, -1$, that belong to the interior of I_h (cf. Fig. 5). We have $f'(x) = 1 + h - 3hx^2$. Then, $f'(0) = 1 + h > 1$, i.e., the fixed point 0 is unstable for any $h > 0$, moreover $f'(1) = f'(-1) = 1 - 2h$, i.e., the fixed points 1 and -1 are stable for $0 < h < 1$ and unstable for $h > 1$. We also have $f'(1) = -1$ and $f'(-1) = -1$ when $h = 1$, hence the two fixed points 1 and -1 undergo a flip bifurcation at $h = 1$ in correspondence to the stability loss. By means of the procedure in [39] we can check that the flip bifurcation is supercritical, hence for h slightly larger than 1 there is a stable 2-cycle encircling the unstable fixed point 1 and another one encircling -1.

Figure 7 shows the bifurcation diagram of f obtained by varying h and starting with an initial condition close to the fixed point 1 (black branch) and the symmetric diagram obtained starting close to the fixed point -1 (red branch). The diagram shows, as predicted, a supercritical flip bifurcation at $h = 1$ originating a stable 2-cycle. This cycle undergoes a second flip bifurcation at $h = 1.236$ with the birth of a stable 4-cycle. Then, a typical cascade of period-doubling bifurcations occurs originating a complex attractor. Analogous considerations hold for the red branch. Figure 8 shows some attractors obtained for specific values of parameter h.

Next, we look for snap-back repellers at the unstable fixed point 0 for $h > 0$ and also at snap-back repellers at the unstable fixed points 1 and -1 for any $h \in (1, 2]$. To address this issue, we find it useful to identify some relevant points in the bifurcation diagram of Fig. 7. Function f vanishes at points 0 and $\pm\sqrt{1 + 1/h}$. Firstly, consider the equation $M(h) = \sqrt{1 + 1/h}$ or

$$f(M(h)) = f(\sqrt{1 + 1/h}) = 0.$$

Taking into account (13), we can recast such equation as

$$\frac{2}{3} \frac{(1+h)^{5/2}}{(3h)^{1/2}} \left[1 - \frac{4}{27}(1+h)^2 \right] = 0$$
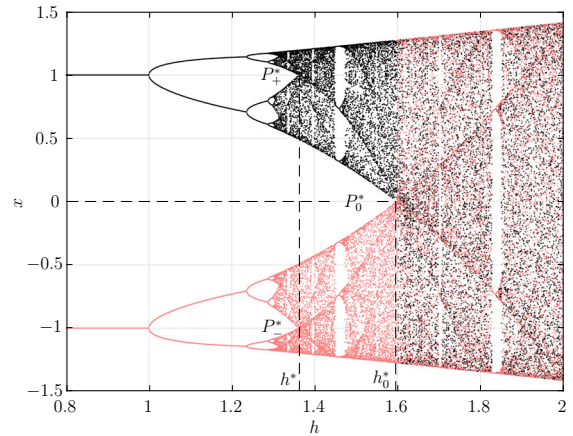

Fig. 7 Bifurcation diagram of the map (12) ($Q_0 = 0$). The black (resp. red) branch is obtained by starting iterates close to 1 (resp., -1). The value $h^* = 1.362$ corresponds to the point P_+^* (resp., P_-^*) where two relevant sub-branches of the black (resp., red) diagram merge with each other. There is a snap-back repeller at the fixed points 1 and -1 when $h > h^*$. The value $h_0^* = 1.598$ corresponds instead to the point P_0^* where the black and red diagram merge. There is a snap-back repeller at the fixed point 0 when $h > h_0^*$. (Color figure online)
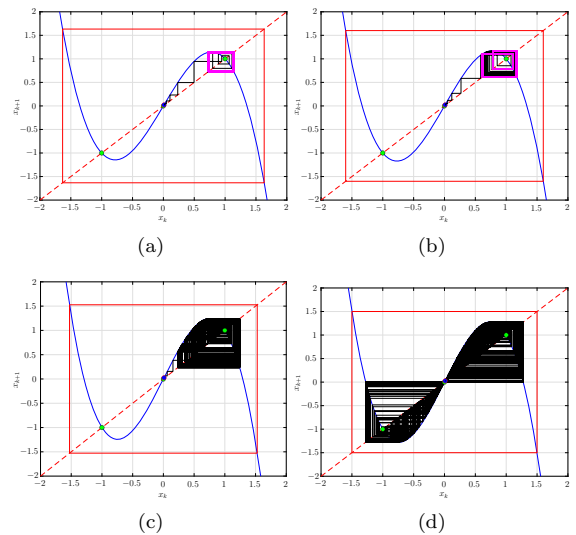

Fig. 8 Forward iterates of map (12) for different values of h. **a** 2-cycle for $h = 1.2$; **b** 4-cycle for $h = 1.28$; **c** single-scroll attractor encircling the fixed point 1 for $h = 1.5$ and **d** double-scroll attractor encircling the fixed points 1 and -1 for $h = 1.6$. (Color figure online)

whose solution in the interval $h \in (1, 2]$ is

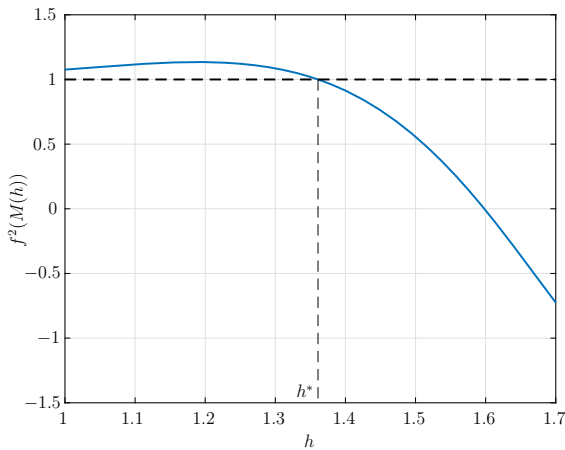$$h_0^* = \frac{3}{2}\sqrt{3} - 1 \simeq 1.598$$

Fig. 9 Curve $f^2(M(h))$ as a function of h for map (12) (blue) in the interval $1 < h \leq 2$. The curve assumes the value 1 at $h^* = 1.362$. (Color figure online)

and it corresponds to the point P_0^* in the bifurcation diagram. It is seen that if $h < h_0^*$, then the intervals $J_+ = [0, \sqrt{1 + 1/h}]$ and $J_- = [-\sqrt{1 + 1/h}, 0]$ are positively invariant, i.e., $f(J_+) \subset J_+$ and $f(J_-) \subset J_-$. Therefore, the iterates starting in J_+ always stay in J_+ and do not intersect J_- and conversely. This corresponds to the fact that the black and red branches do not intersect for $h < h_0^*$. Instead, when $h > h_0^*$ the intervals J_+ and J_- are no longer positively invariant and iterates may switch between these two intervals. For $h > h_0^*$ there is indeed a drastic change in the dynamics since the black and red branches of the diagram merge, namely, the scroll around the fixed point 1 merges with that around the fixed point -1 and they give birth to a double-scroll attractor encircling both fixed points 1 and -1 (Fig. 8).

Let us now consider the equation

$$f^2(M(h)) = 1.$$

As it can be seen from Fig. 9, this equation has a solution $h^* = 1.362$ in the interval $1 < h \leq 2$. The value h^* corresponds to the point we denoted by P_+^* (resp., P_-^*) in the bifurcation diagram of Fig. 7 where two relevant subbranches of the black (resp., red) branch merge with each other.

The special values h_0^* and h^* thus singled out have an important meaning, as it is shown in the next result.

Theorem 1 *For any $h \in (h_0^* = 1.598, 2]$ the first-order map (12) has a snap-back repeller at the fixed point 0. Moreover, for any $h \in (h^* = 1.362, 2]$ the same map has a snap-back repeller at the fixed points 1 and -1.*

Proof Snap back repeller at fixed point 0. Suppose $h > h_0^* = 1.598$, in which case $f'(0) > 1$ and the fixed point 0 is unstable. We wish to verify the existence of a snap-back repeller at 0 by means of Definition 3. To this end, first we need an estimate of the neighborhood $B_r(0) = \{x : |x| \leq r\}$ of 0 where $f'(x) > 1$ for any $x \in B_r(0)$. It turns out that a suitable choice is $r < 1/\sqrt{3}$, for instance, $r = 0.577$.

Next, we have to find (if it exists) a point $z_0 \in B_r(0)$, $z_0 \neq 0$, and a positive integer m such that $f^m(z_0) = 0$ and $(f^m)'(z_0) \neq 0$. To accomplish this task, as it is discussed next, it is convenient to study the pre-images $F^{-m}(0)$ of the fixed point 0. By construction we have $f(I_h) = I_h$. Since f is not injective, in general there is more than one pre-image $F^{-1}(y)$ of a point $y \in I_h$. Indeed, it is seen that there are from 1 to 3 pre-images of $y \in I_h$. We will consider this strategy to construct in a unique way a sequence of pre-images $f^{-1}(0), f^{-2}(0), \ldots, f^{-k}(0)$, $k = 3, 4, \ldots$, of the fixed point 0, all of which belong to I_h. The pre-image $f^{-1}(0)$ is chosen as the smallest (negative) solution of $f(x) = 0$. Since $h > h_0^* = 1.598$, we have $-M(h) < f^{-1}(0)$ and there are 3 pre-image candidates for $f^{-2}(0)$. In this case, we will choose the intermediate (central) pre-image (cf. Fig. 10). Note that $-x_M \leq f^{-2}(0) < 0$, where $-x_M = \arg\min_{x \in (-\infty, 0]}(f) = -\sqrt{(1 + h)/(3h)}$. If $f^{-2}(0) \in B_r(0)$ the proof is completed with $m = 2$. Otherwise, we choose the central pre-image also for $f^{-3}(0)$, and we will prove that $f^{-3}(0) \in B_r(0)$. Indeed, first note that $x - f(x) = hx(x^2 - 1) \geq 0$ for any $x \in (-1, 0)$, thus implying that $-1 < -x_M < f^{-2}(0) \leq f^{-3}(0) < 0$. Also, consider the quantity $\Delta f(f^{-2}(0)) = f^{-2}(0) - f(f^{-2}(0)) = hf^{-2}(0)((f^{-2}(0))^2 - 1)$, which describes the size of the step $f^{-3}(0) - f^{-2}(0)$. It can be checked that this is an increasing function whenever $f^{-2}(0) \in (-x_M, 1/\sqrt{3})$, while it decreases when $f^{-2}(0) \in (1/\sqrt{3}, 0)$. Since we have assumed $f^{-2}(0) \notin B_r(0)$, we have $-x_M \leq f^{-2}(0) \leq -1/\sqrt{3}$, so we can write the following inequality

$$f^{-3}(0) = f^{-2}(0) + \Delta f(f^{-2}(0)) \geq -x_M + \Delta f(-x_M)$$
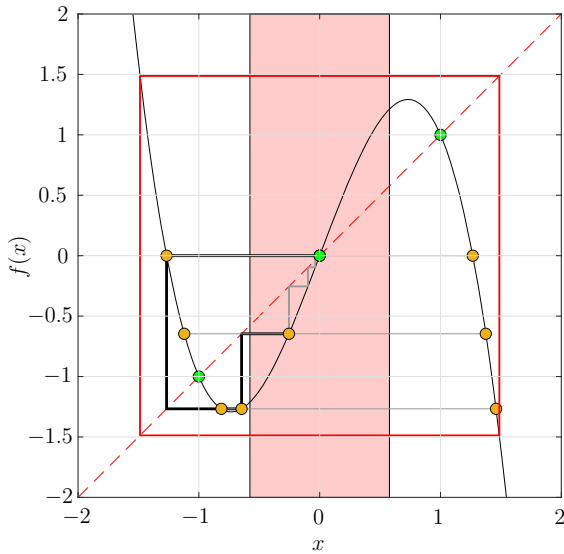$$= \sqrt{\frac{1 + h}{3h}} \left(\frac{2h - 4}{3} \right).$$

Fig. 10 Backward iterates $f^{-1}(0)$, $f^{-2}(0)$ and $f^{-3}(0)$ of map (12) when $h = 1.4 > h_0^*$. Also shown is $B_r(0)$ (rose). (Color figure online)

Fig. 11 Behavior as a function of h of backward iterates $|f^{-1}(0)|$ (blue), $|f^{-2}(0)|$ (red) and $|f^{-3}(0)|$ (green) of map (12). The dashed black line represents the value $r = 1/\sqrt{3}$. (Color figure online)

Since $h > h_0^* = 1.598$, we obtain $0 > f^{-3}(0) > -0.19 > -1/\sqrt{3}$, i.e., $f^{-3}(0) \in B_r(0)$. Since no selected pre-image coincides with $-x_M$, then

$$(f^3)'(z_0) = \prod_{k=1}^{3} f'(f^{-k}(0)) \neq 0.$$

As an illustration, Fig. 11 shows the values of backwards iterates $f^{-1}(0)$, $f^{-2}(0)$ and $f^{-3}(0)$ as a function of h. It can be checked that, for any $h \in (h_0^*, 2]$, we have $z_0 = f^{-3}(0) \in B_r(0) \backslash \{1\}$, $z_0 \neq 0$, i.e., 0 is mapped back to a point in $B_r(0)$ in $m = 3$ backward iterates. This concludes the first part of the proof.

Snap back repeller at fixed points 1 and -1. Next, we study snap-back repellers at the fixed point 1 but for symmetry reasons the obtained results also hold for the fixed point -1. Suppose $h > h^* = 1.362$, in which case $f'(1) < -1$ and the fixed point 1 is unstable. Consider the definition of a snap-back repeller for fixed point 1 (Definition 3). First, we need an estimate of the neighborhood $B_r(1) = \{x : |x - 1| \leq r\}$ of 1 where $f'(x) < -1$ for any $x \in B_r(1)$. It can be shown that a suitable choice is

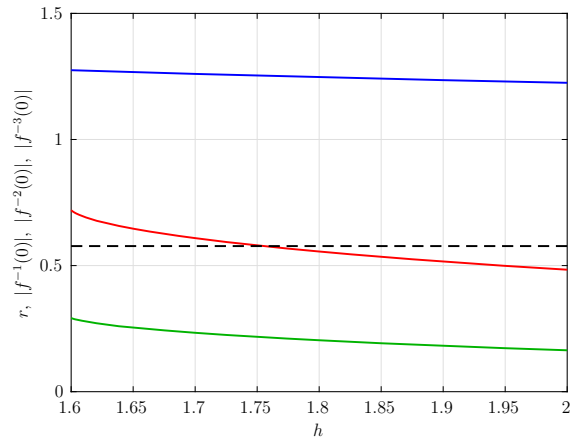$$r = r(h) = 1 - \sqrt{\frac{h+2}{3h}}.$$

Since

$$r'(h) = \frac{2}{3} \frac{1}{\sqrt{\frac{h+2}{3h}} h^2} > 0$$

it follows that $r(h)$ is an increasing function of h assuming values between 0 ($h = 1$) and 0.18 ($h = 2$).

Next, we have to find (if it exists) a point $z_0 \in B_r(1)$, $z_0 \neq 1$, and a positive integer m such that $f^m(z_0) = 1$ and $(f^m)'(z_0) \neq 0$. Let us study the pre-images $F^{-m}(1)$ of the fixed point 1. We will consider this strategy to construct in a unique way a sequence of inverse images $f^{-1}(1), f^{-2}(1), \ldots, f^{-k}(1)$, $k = 3, 4, \ldots$, of the fixed point 1, all of which belong to I_h. The pre-image $f^{-1}(1)$ is chosen as the largest solution of $f(x) = 1$ except for the fixed point 1, i.e., $f^{-1}(1) = \sup\{F^{-1}(1)\backslash\{1\}\}$. Thereafter, $f^{-n}(1)$ is chosen as the largest positive solution of $f(x) = f^{-(n-1)}(1)$, i.e., we have $f^{-n}(1) = \sup F^{-(n-1)}(1)$, for $n = 2, 3, \ldots$, see Fig. 12 for an illustration. Now, suppose we are able to find m such that $z_0 = f^{-m}(1) \in B_r(1)$, $z_0 \neq 1$ and also $f'(f^{-k}(1)) \neq 0$, $k = 1, \ldots, m$. Then, z_0 is the point we are looking for in the definition of a snap-back repeller. In fact, we have $f^m(z_0) = 1$ and also $(f^m)'(z_0) = \prod_{k=1}^{m} f'(f^{-k}(1)) \neq 0$.

Figure 13 shows the values of the backwards iterates $f^{-2}(1)$ up to $f^{-5}(1)$ as a function of h. It is seen that, for any $h \in (h^*, 2]$, we have $z_0 = f^{-5}(1) \in B_r(1)\backslash\{1\}$, $z_0 \neq 0$, i.e., z_0 is mapped back to a point in $B_r(1)$ in five backward iterates. Moreover, it can be
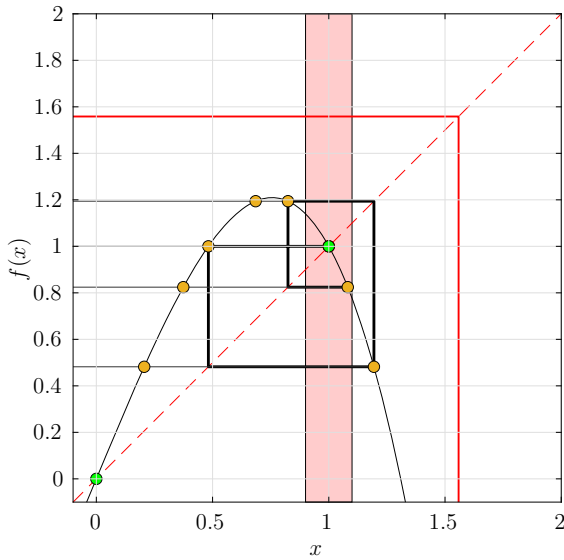
Fig. 12 Backward iterates $f^{-1}(1)$, $f^{-2}(1)$, $f^{-3}(1)$, $f^{-4}(1)$ of map (12) when $h = 1.4 > h^*$. Also shown is $B_r(1)$ (rose). (Color figure online)
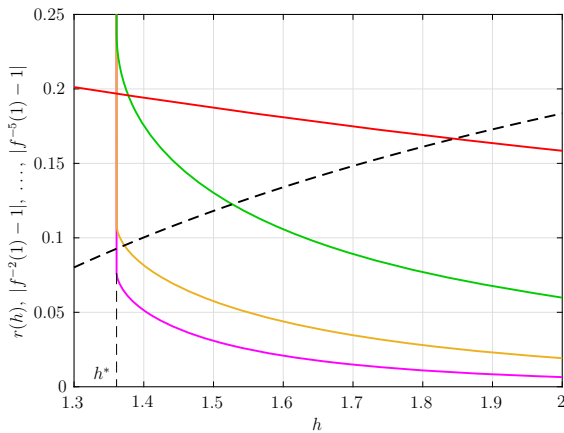

Fig. 13 Behavior as a function of h of $r(h)$ (black) and backward iterates $|f^{-2}(1) - 1|$ (red), $|f^{-3}(1) - 1|$ (green), $|f^{-4}(1) - 1|$ (orange) and $|f^{-5}(1) - 1|$ (violet) of map (12). (Color figure online)

checked that $f'(f^{-k})(1) \neq 0$, $k = 1, 2, \ldots, 5$.[1] This concludes the proof. □

_____
[1] Actually, Fig. 13 shows that for larger values of h we need a lower number of backward iterates. For instance, when $h = 1.5$ we have $f^{-4}(1) \in B_r(1)$, when $h = 1.7$ the iterate $f^{-3} \in B_r(1)$ and when $h = 1.9$ we have $f^{-2}(1) \in B_r(1)$.

4 Snap-back repellers when $Q_0 \neq 0$

Consider now the case where $Q_0 \neq 0$. Since Q_0 is fixed, the map (11), which is rewritten below for convenience

$$x \to f(x) = (1 + h)x - hx^3 + hQ_0 \qquad (15)$$

depends once more upon a single parameter $h > 0$ (the step size). Figure 14 shows f for different values of h. Note that f is no longer symmetric with respect to the origin. Let $M_+(h) = M(h) + hQ_0$ (resp., $M_-(h) = -M(h) + hQ_0$), where $M(h)$ is given in (13), be the maximum (resp., minimum) of f in $[0, +\infty)$ (resp., $(-\infty, 0]$).

To a large extent we can follow a treatment analogous to the case $Q_0 = 0$ to find snap-back repellers at fixed points. However, there are some remarkable differences that are discussed next. The fixed points are the solutions of $-x + x^3 = Q_0$. Depending upon Q_0, there may exist one, two or three different fixed points. Henceforth, we consider the most interesting case where there are three fixed points $\bar{x}_- < \bar{x}_0 < \bar{x}_+$. The range of Q_0 where there are three fixed points can be analytically derived by exploiting the Cardan discriminant, obtaining

$$Q_0 \in \left(-\frac{2\sqrt{3}}{9}, \frac{2\sqrt{3}}{9} \right) \simeq (-0.3849, 0.3849). \qquad (16)$$

It is seen that in the Q_0 range (16) the fixed point $\bar{x}_0 \in (-1/\sqrt{3}, 1/\sqrt{3})$ and it is unstable. Moreover, $\bar{x}_+ \in (1/\sqrt{3}, +\infty)$ and it is stable if

$$\bar{x}_+ \in (1/\sqrt{3}, \sqrt{(2 + h)/3h})$$

and unstable if

$$\bar{x}_+ \in (\sqrt{(2 + h)/3h}, +\infty).$$

We have a flip bifurcation at $\bar{x}_+ = \sqrt{(2 + h)/3h}$. Similarly, $\bar{x}_- \in (-\infty, -1/\sqrt{3})$ and it is stable if

$$\bar{x}_- \in (-\sqrt{(2 + h)/3h}, -1/\sqrt{3})$$

and unstable whenever we have
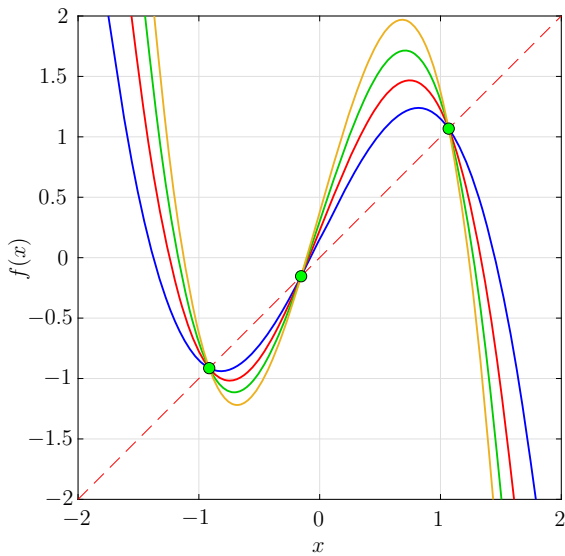
$$\bar{x}_- \in (-\infty, -\sqrt{(2 + h)/3h}).$$

Fig. 14 Behavior of f for the map (15) when $h = 1$ (blue), $h = 1.5$ (red), $h = 2$ (green) and $h = 2.5$ (orange) and $Q_0 = 0.15$. The three fixed points $\bar{x}_-$, $\bar{x}_0$ and $\bar{x}_+$ are marked by green points. (Color figure online)

Fig. 15 Curve $h_{\max}(Q_0)$ (black) delimiting the region in the plane (h, Q_0) where I_h is invariant for the map (15). Also shown are the four curves $h_-^j(Q_0)$ (green), $h_+^j(Q_0)$ (violet), $h_+^*(Q_0)$ (red) and $h_-^*(Q_0)$ (blue), that delimit regions in the plane (h, Q_0) where there exist snap-back repellers at the fixed point $\bar{x}_-$, denoted by -1, $\bar{x}_0$, denoted by 0 and $\bar{x}_+$, denoted by 1. The horizontal dashed lines correspond to the special cases $Q_0 = 0.05$ and $Q_0 = 0.15$. (Color figure online)

We have a flip bifurcation at $x_- = -\sqrt{(2 + h)/3h}$.

We can find an invariant interval for (15) via a straightforward generalization of the procedure for $Q_0 = 0$. Let $\alpha_+(h)$ (resp., $\alpha_-(h)$) be the maximal (resp., minimal) solution of $f^2(x) = x$.

Proposition 2 *The following hold.*

(i) For any $h > 0$ we have $\alpha_+(h) > \bar{x}_+$, and $\alpha_-(h) < \bar{x}_-$. Moreover, $(f^2)'(\alpha_+(h)) > 1$, i.e., the 2-cycle $\alpha_+(h) \to \alpha_-(h) \to \alpha_+(h)$ is unstable.

(ii) If

$$\alpha_+(h) \geq M_+(h), \quad \alpha_-(h) \leq M_-(h) \tag{17}$$

then

$$I_h \doteq [\alpha_-(h), \alpha_+(h)]$$

is an invariant interval for the map (15), i.e., $f(I_h) = I_h$.

Proof The proof is similar to that of Proposition 1 and is omitted for brevity. □

It turns out that condition (17) is satisfied, hence the interval I_h is invariant for the map (15), for any $h \in (0, h_{\max}(Q_0)]$, where $h_{\max}(Q_0)$ is the curve shown in black in Fig. 15.
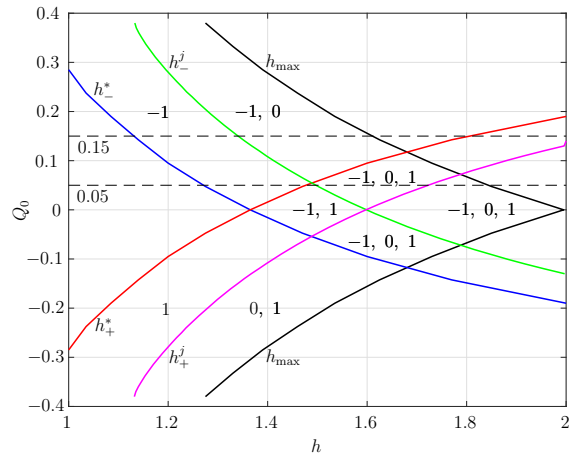
In analogy to what has been done before, let us identify for any Q_0 some relevant values of h in the bifurcation diagram. First, consider the curve $h_-^j(Q_0)$ (resp., $h_+^j(Q_0)$), obtained by solving the equation $f(M_+(h)) = \bar{x}_0$ (resp., $f(M_-(h)) = \bar{x}_0$). Moreover, consider the curve $h_+^*(Q_0)$ obtained by solving $f^2(M_+(h)) = \bar{x}_+$ and the curve $h_-^*(Q_0)$ found by solving $f^2(M_-(h)) = \bar{x}_-$. The curves are shown in Fig. 15. On this basis, we can identify regions in the parameter plane (h, Q_0) where snap-back repellers at the fixed points $\bar{x}_-$, $\bar{x}_0$ and $\bar{x}_+$ can be found (see Fig. 15). For example, in the region denoted with 0, 1, there is a snap-back repeller at $\bar{x}_0$ and $\bar{x}_+$. Next, we explain in more detail the obtained results by analyzing the two special cases $Q_0 = 0.05$ and $Q_0 = 0.15$. An analogous treatment can be repeated for any other value of Q_0.

4.1 Snap-back repellers when $Q_0 = 0.05$

Suppose that $Q_0 = 0.05$. We have $\bar{x}_- = -0.974$, $\bar{x}_0 = -0.050$ and $\bar{x}_+ = 1.024$. The fixed point $\bar{x}_0$ is unstable, whereas $\bar{x}_+$ (resp., $\bar{x}_-$) is stable for $h < 0.931$ (resp., $h < 1.083$) and unstable for $h > 0.931$ (resp., $h > 1.083$). Point $\bar{x}_+$ (resp., $\bar{x}_-$) undergoes a supercritical
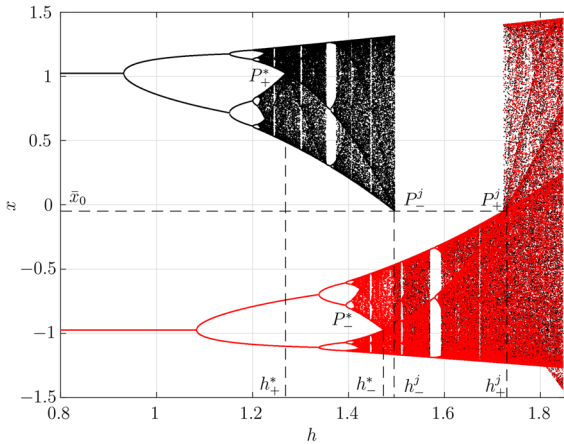
Fig. 16 Bifurcation diagram of the map (15) when $Q_0 = 0.05$. The black (resp. red) branch is obtained by starting close to $\bar{x}_+ = 1.024$ (resp., to $\bar{x}_- = -0.974$). The value $h_-^j = 1.495$ (resp., $h_+^j = 1.726$) corresponds to the point P_-^j (resp., P_+^j) where there is a negative (resp., positive) jump from the black (resp., red) branch of the diagram to the red (resp., black) branch. There is a snap-back repeller at $\bar{x}_0$ when $h > h_-^j$. The value $h_+^* = 1.269$ (resp., $h_-^* = 1.474$) corresponds to the point P_+^* (resp., P_-^*). There is a snap-back repeller at $\bar{x}_+$ (resp., $\bar{x}_-$) when $h > h_+^* = 1.269$ (resp., $h > h_-^* = 1.474$). (Color figure online)

flip bifurcation at $h = 0.931$ (resp., $h = 1.083$). Note that we have an asymmetric situation where $\bar{x}_+$ loses stability before $\bar{x}_-$ as h increases.

The bifurcation diagram for $Q_0 = 0.15$ and $0 < h < h_{\max}(Q_0 = 0.05) = 1.85$ is shown in Fig. 16. Once more there are two main branches, one obtained starting close to $\bar{x}_+$ (black) and one obtained starting close to $\bar{x}_-$ (red). Now, the two branches are asymmetric since f is no longer symmetric as in the case $Q_0 = 0$. One main difference with respect to the case $Q_0 = 0$ is that at $h_-^j = 1.495$ (cf. Fig. 15), we observe a negative jump from the black toward the red branch. This can be explained as follows. Consider the intervals J_+ and J_- shown in Fig. 17. We have that $f(J_+) \subset J_+$, i.e., J_+ is positively invariant, up to $h_-^j = 1.495$, while for $h > h_-^j$ we have $f(J_+) \not\subset J_+$ and iterations starting in J_+ reach a sufficiently large amplitude and they can switch down to J_-. Similarly, J_- is positively invariant up to $h_+^j = 1.726$, while for $h > h_+^j$ iterations staring in J_- can switch up to J_+. Therefore, in the range $h_-^j < h < h_+^j$ the iterations starting close to $\bar{x}_+$ get stuck into the attraction basin of the complex attractor corresponding to the red branch. For larger values of h, i.e., $h > h_+^j$, also the oscillations starting close to
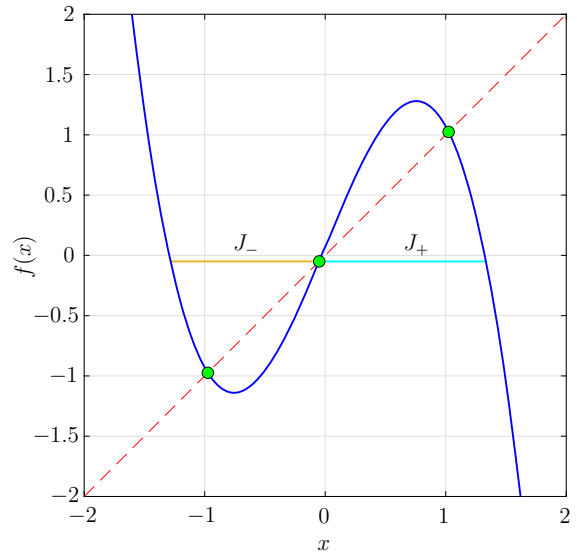

Fig. 17 Behavior of f for the map (15) when $h = 1.4$ and intervals $J_- = [-1.295, x_0 = -0.0501]$ and $J_+ = [x_0 = -0.0501, 1.324]$. (Color figure online)
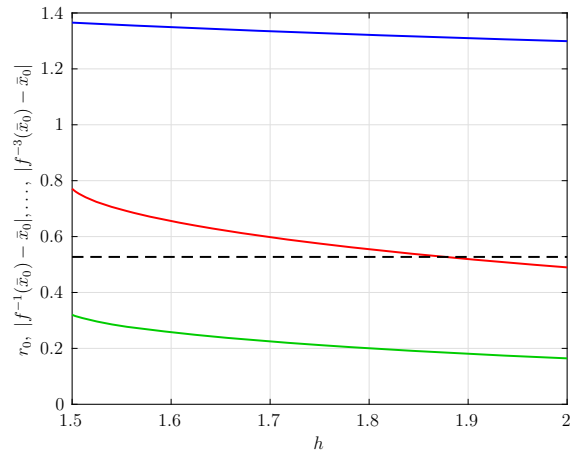

Fig. 18 Behavior as a function of h of backward iterates $|f^{-1}(\bar{x}_0) - \bar{x}_0|$ (blue), $|f^{-2}(\bar{x}_0) - \bar{x}_0|$ (red) and $|f^{-3}(\bar{x}_0) - \bar{x}_0|$ (green) of map (15) when $Q_0 = 0.05$. The dashed black line represents the value $r_0 = |1/\sqrt{3} - |\bar{x}_0|| = 0.526$. (Color figure online)

$\bar{x}_-$ reach a sufficiently large amplitude to merge with those starting close to x_+. This gives rise to a double scroll attractor encircling both fixed points $\bar{x}_-$ and $\bar{x}_+$.

Now, we look for snap-back repellers at the fixed points $\bar{x}_-$, $\bar{x}_0$ and $\bar{x}_+$. First, consider $\bar{x}_0$. Let r_0 be such that $f'(x) > 1$ in $B_{r_0}(\bar{x}_0)$. We have that $r_0 = |1/\sqrt{3} - |\bar{x}_0|| \simeq 0.526$ is a constant independent of h, as shown in Fig. 18. The same figure shows the backward
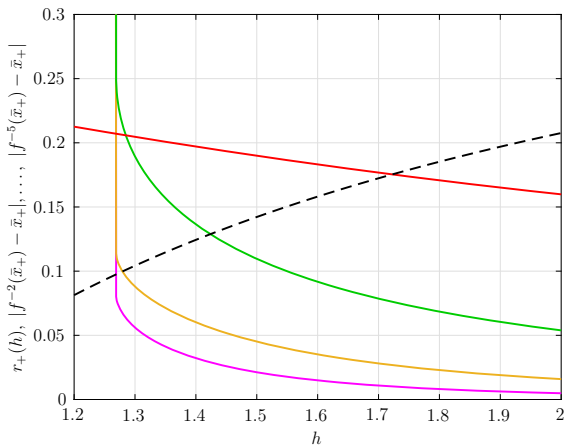
Fig. 19 Behavior as a function of h of $r_+(h)$ (black) and backward iterates $|f^{-2}(\bar{x}_+) - \bar{x}_+|$ (red), $|f^{-3}(\bar{x}_+) - \bar{x}_+|$ (green), $|f^{-4}(\bar{x}_+) - \bar{x}_+|$ (orange) and $|f^{-5}(\bar{x}_+) - \bar{x}_+|$ (violet) of map (15) when $Q_0 = 0.05$. (Color figure online)
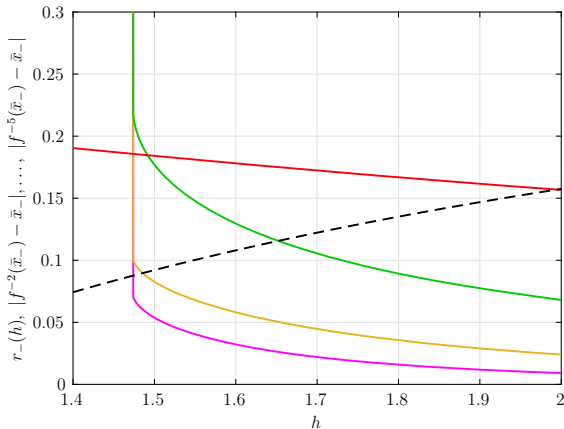

Fig. 20 Behavior as a function of h of $r_-(h)$ (black) and backward iterates $|f^{-2}(\bar{x}_-) - \bar{x}_-|$ (red), $|f^{-3}(\bar{x}_-) - \bar{x}_-|$ (green), $|f^{-4}(\bar{x}_-) - \bar{x}_-|$ (orange) and $|f^{-5}(\bar{x}_-) - \bar{x}_-|$ (violet) of map (15) when $Q_0 = 0.05$. (Color figure online)

iterates $f^{-1}(\bar{x}_0)$, $f^{-2}(\bar{x}_0)$ and $f^{-3}(\bar{x}_0)$ as a function of h. These are constructed with a procedure analogous to that used for the fixed point 0 in the case $Q_0 = 0$. It is seen that for any $h > h_-^j$, $f^{-3}(\bar{x}_0) \in B_{r_0}(\bar{x}_0)$, hence for these values of h the map (15) has a snap-back repeller at $\bar{x}_0$ (cf. Fig. 15).

Now, consider the fixed point $\bar{x}_+$ (resp., $\bar{x}_-$) and let r_+ be such that $f'(x) < -1$ in $B_{r_+}(\bar{x}_+)$ (resp., in $B_{r_-}(\bar{x}_-)$). Figure 19 (resp., Fig. 20) shows $r_+(h)$ (resp., $r_-(h)$) and the iterates $f^{-2}(\bar{x}_+), \ldots, f^{-5}(\bar{x}_+)$ (resp., $f^{-2}(\bar{x}_-), \ldots, f^{-5}(\bar{x}_-)$) as a function of h. We conclude that, for any $h > h_+^* = 1.269$ (resp., $h >$
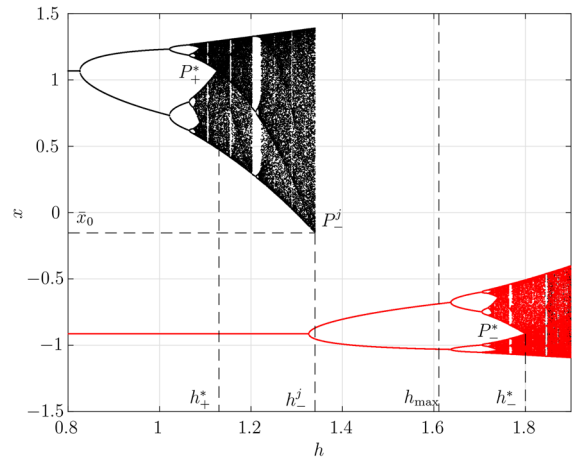

Fig. 21 Bifurcation diagram of (15) when $Q_0 = 0.15$. The black (resp. red) branch is obtained by starting close to $\bar{x}_+ = 1.068$ (resp., to $\bar{x}_- = -0.914$). The value $h_-^j = 1.340$ corresponds to the point P_-^j where there is a negative jump from the black branch of the diagram to the red branch. A snap-back repeller at $\bar{x}_0$ is present when $h > h_-^j$. The value $h_+^* = 1.126$ (resp., $h_-^* = 1.801$) corresponds to the point P_+^* (resp., P_-^*). There is a snap-back repeller at $\bar{x}_+$ (resp., $\bar{x}_-$) when $h > h_+^*$ (resp., $h > h_-^*$). The vertical straight line at $h_{\max}(Q_0) = 1.611$ delimits the region where all iterates starting in I_h are bounded ($h < h_{\max}(Q_0)$) from the region where iterates starting in I_h may grow unboundedly ($h > h_{\max}(Q_0)$). (Color figure online)

$h_-^* = 1.474$), we have $f^{-5}(\bar{x}_+) \in B_{r_+}(\bar{x}_+)$ (resp., $f^{-5}(\bar{x}_-) \in B_{r_-}(\bar{x}_-)$), hence for these values of h the map (15) has a snap-back repeller at $\bar{x}_+$ (resp., $\bar{x}_-$). Again, see Fig. 15.

4.2 Snap-back repellers when $Q_0 = 0.15$

Suppose that $Q_0 = 0.15$. We have $\bar{x}_- = -0.914$, $\bar{x}_0 = -0.154$ and $\bar{x}_+ = 1.068$. The fixed point $\bar{x}_0$ is unstable, whereas $\bar{x}_+$ (resp., $\bar{x}_-$) is stable for $h < 0.825$ (resp., $h < 1.323$) and unstable for $h > 1.323$ (resp. $h > 0.825$). The fixed point $\bar{x}_+$ (resp., $\bar{x}_-$) undergoes a supercritical flip bifurcation at $h = 0.825$ (resp., $h = 1.323$). Again, we have an asymmetric situation where $\bar{x}_+$ loses stability before $\bar{x}_-$ as h increases.

The bifurcation diagram for $Q_0 = 0.15$ is shown in Fig. 21. Once more there are two main asymmetric branches, one obtained starting close to $\bar{x}_+$ (black) and one obtained starting close to $\bar{x}_-$ (red). At $h_-^j = 1.340$ (cf. Fig. 15), we observe a negative jump from the black toward the red branch, which can be explained arguing as in the case $Q_0 = 0.05$. Notice that we

have $h_{\max}(Q_0 = 0.15) = 1.611$, while the bifurcation diagram is shown up to $h = 1.9 > h_{\max}(Q_0)$. Actually, when $h < h_{\max}(Q_0)$, I_h is invariant and iterations starting in I_h are bounded. Instead, when $h_{\max}(Q_0) < h < 1.9$, I_h is no longer positively invariant and some iterations starting in I_h may grow unboundedly. Nevertheless, we have found numerically that iterations starting close to $\bar{x}_-$ are bounded also when $h_{\max}(Q_0) < h < 1.9$, as it can be seen in the portion of the red branch corresponding to these values of h.

It has been checked that for $Q_0 = 0.15$ is a snap-back repeller at $\bar{x}_0$ when $h > h_-^j = 1.340$. Moreover, there is a snap-back repeller at $\bar{x}_+$ (resp., $\bar{x}_-$) when $h > h_+^* = 1.126$ (resp., $h > h_-^* = 1.801$) (details are omitted).

5 Discussion

In this section, we provide some remarks on the results obtained for the maps of DT-MCC.

1. We have seen in Sect. 2 that, due to the existence of a first integral, the state space of a DT-MCC in the VCD can be foliated in invariant manifolds and on each manifold the dynamics in the FCD is described by a first-order map depending upon the manifold index Q_0 or, equivalently, upon the initial conditions in the VCD. Then, in Sects. 3 and 4 it has been shown that for any $Q_0 \in (-0.3849, 0.3849)$ there are ranges of parameter h (cf. Fig. 15) where DT-MCC has snap-back repellers and therefore it displays chaos in the Marotto and also in the Li–Yorke sense when DT-MCC evolves in the corresponding manifold. Moreover, changing Q_0 and the manifold implies changes in the bifurcation diagrams and the generated chaos as detailed in the particular cases $Q_0 = 0.05$ and $Q_0 = 0.15$. We stress that all these infinitely many different chaotic behaviors coexist for the same set of circuit parameters of DT-MCC, i.e., DT-MCC displays extreme multistability.

2. In Sects. 3 and 4 we analyzed snap-back repellers of the map (10) in the special, yet typical case where the parameters of the memristor nonlinearity $q_M = \hat{q}(\varphi_M) = -a\varphi_M + b\varphi_M^3$ are chosen as $a = b = 1$. Actually, an analogous treatment and similar results are obtained if we consider any locally-active memristor with $a, b > 0$. As an example, if we choose another typical set of values, i.e., $a = 1$ and $b = 1/3$, we obtain for snap-back repellers the scenario shown in Fig. 22 for
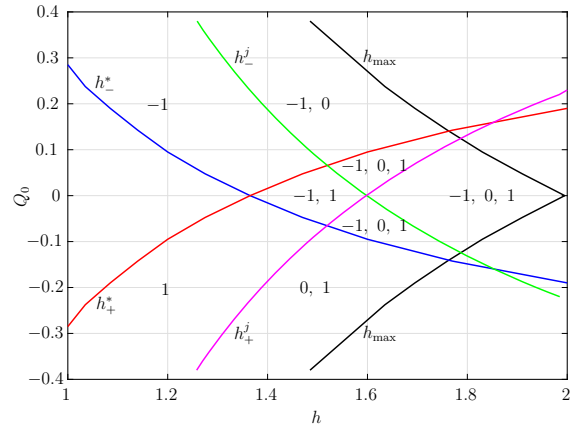

Fig. 22 Curve $h_{\max}(Q_0)$ (black) delimiting the region in the plane (h, Q_0) where I_h is invariant for the map (10) with $a = 1$, $b = 1/3$. Also shown are the four curves $h_-^j(Q_0)$ (green), $h_+^j(Q_0)$ (violet), $h_+^*(Q_0)$ (red) and $h_-^*(Q_0)$ (blue), that delimit regions in the plane (h, Q_0) where there exist snap-back repellers at the fixed point $\bar{x}_-$, denoted by -1, $\bar{x}_0$, denoted by 0, and $\bar{x}_+$, denoted by 1. (Color figure online)

map (10), which is qualitatively similar to that of Fig. 15. Finally, Fig. 23 shows the bifurcation diagram of the same map when $Q_0 = 0$. This diagram is remarkably similar to that obtained in the case $a = b = 1$ (cf. Fig. 7). Note that the horizontal segments for $h \leq 1$ in the two diagrams are different. This is because the fixed points $\pm\sqrt{a/b}$ of the map (9) for $Q_0 = 0$ depend upon parameter b. On the contrary, the values $h^* = 1.362$ and $h_0^* = 1.598$ in the diagrams coincide. This follows from the fact that, as it is shown in the Appendix, we have

$$h^*(a, b) = \frac{1}{a}h^*(1, 1); \quad h_0^*(a, b) = \frac{1}{a}h_0^*(1, 1)$$

where (Sect. 3)

$$h^*(1, 1) = 1.362; \quad h_0^*(1, 1) = \frac{3}{2}\sqrt{3} - 1 \simeq 1.598.$$

3. Let us consider the DT-MCC map (11) in the special case where $Q_0 = 0$ and $h = 2$, i.e.,

$$x \to f(x) = 3x - 2x^3. \tag{18}$$

The graph of f is shown in Fig. 24a. We can subdivide the interval $I_h = [-\alpha(h), \alpha(h)] = [-1.414, 1.414]$ in three subintervals
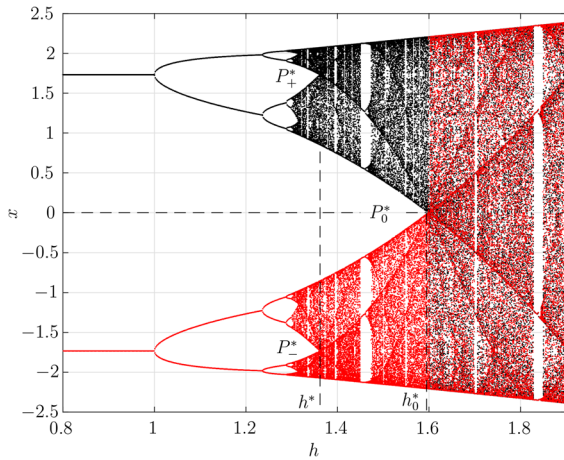
Fig. 23 Bifurcation diagram of the map (10) when $a = 1$, $b = 1/3$ and $Q_0 = 0$. The black (resp. red) branch is obtained by starting iterates close to 1 (resp., -1). The value $h^* = 1.362$ corresponds to the point P_+^* (resp., P_-^*) where two relevant subbranches of the black (resp., red) diagram merge with each other. There is a snap-back repeller at the fixed points 1 and -1 when $h > h^*$. The value $h_0^* = 1.598$ corresponds instead to the point P_0^* where the black and red diagram merge. There is a snap-back repeller at the fixed point 0 when $h > h_0^*$. (Color figure online)

$$J_a = [-\alpha(h), \sqrt{(1+h)/3h}] = [-1.414, -0.707],$$

$$J_b = [-\sqrt{(1+h)/3h}, \sqrt{(1+h)/3h}]$$
$$= [-0.707, 0.707]$$

and

$$J_c = [\sqrt{(1+h)/3h}, \alpha(h)] = [0.707, 1.414],$$

such that $I_h = J_a \cup J_b \cup J_c$, each restriction $J_a \to f(J_a)$, $J_b \to f(J_b)$ and $J_c \to f(J_c)$ is a homeomorphism and moreover $f(J_a) = f(J_b) = f(J_c) = I_h$. If we consider f^2, then its graph in each subinterval reproduces that of f on I_h (Fig. 24b). In a similar way we can construct the graphs of successive iterates $f^3, f^4, \ldots, f^n$, see, e.g., Fig. 24c, d for the graph of f^3 and f^4. It can be checked that there are 9 intersections of f^2 with the line $y = x$ so that, excluding fixed points, there are three 2-period cycles. Moreover, there are 27 intersections of f^3 with $y = x$ and then, excluding fixed points, there are eight 3-period cycles (Fig. 24c), while there are 81 intersections of f^4 with $y = x$ and so, excluding fixed points and 2-period cycles, there are eighteen 4-period cycles (Fig. 24d).
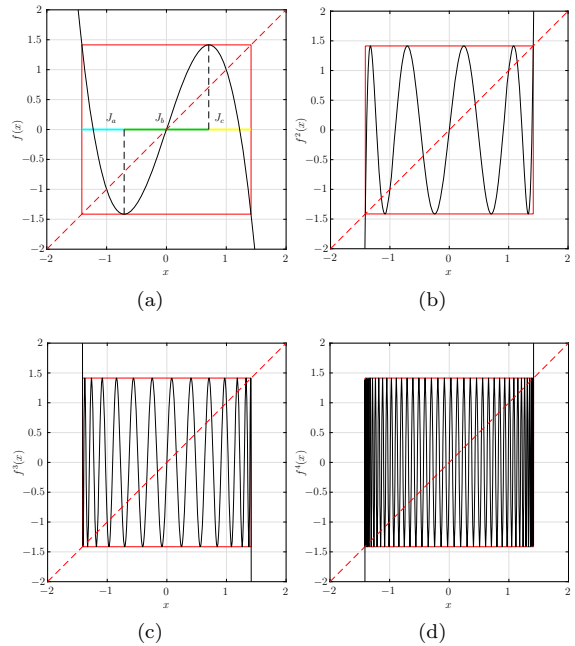

Fig. 24 Case $Q_0 = 0$ and $h = 2$. Graph of **a** f; **b** f^2; **c** f^3 and **d** f^4. (Color figure online)

Arguing in a similar way for f^n we can conclude that there are n-period cycles for any positive integer $n > 4$. On one hand this is accordance with the existence of snap back repellers for the map (18). On the other hand, it is also in agreement with Li–Yorke theorem [40] and Sharkovskii theorem [43], according to which the existence of a 3-period cycle implies the existence of n-period cycles for any $n \geq 2$.

6 Conclusion

The paper has considered a class of DT memristor circuits that possess invariants of motion and display an initial condition dependent dynamics showing extreme multistability and bifurcations without parameters. The paper used analytic tools for a thorough and rigorous investigation of chaos in this class of DT memristor circuits. In particular, parameter ranges are identified where the DT circuits have snap-back repellers at fixed points and they display chaos in the Marotto and also in the Li–Yorke sense. Bifurcations diagrams are provided and relevant points on these diagrams identifying the birth of snap-back repellers and the onset of chaos are highlighted. The paper has also studied how the bifurcation diagrams and snap-back repellers depend

upon the specific manifold and the circuit initial conditions. We believe the techniques here described are potentially useful to study chaos also in other classes of DT memristor circuits. This will be the subject of future work on this topic.

Declarations

Appendix

Consider the case $Q_0 = 0$, $a, b > 0$. The values of $h_0^*(a, b)$ and $h^*(a, b)$ are obtained by solving the equations

$$f(M(h_0^*(a, b)) = x_0 \tag{19}$$

and

$$f^2(M(h^*(a, b)) = x_+ \tag{20}$$

respectively, where $x_0 = 0$, $x_+ = \sqrt{a/b}$, are the fixed points of (10), while

$$M(h) = g_0(ah)x_z \tag{21}$$

where $g_0(ah) = (2/(3\sqrt{(3)}))(1 + ah)$ and the value $x_z = \sqrt{(1 + ah)/(hb)}$ is such that $f(x_z) = 0$. This yields that (19) is indeed equivalent to $M(h_0^*(a, b)) = x_z$ and thus, taking into account (21), it boils down to

$$\frac{2}{3\sqrt{3}}(1 + ah_0^*(a, b)) = 1$$

which implies

$$h_0^*(a, b) = \frac{1}{a}\left(\frac{3\sqrt{3}}{2} - 1\right) = \frac{1}{a}h_0^*(1, 1).$$

Now, considering (21), after some straightforward manipulation, we have

$$f(M(h^*(a, b))) = g_1(ah^*(a, b))x_z$$

where g_1 is a function of ah. Following the same reasoning, we have that there exists a suitable function $g_2(ah)$ such that

$$f^2(M(h^*(a, b))) = g_2(ah^*(a, b))x_z.$$

Then, (20) boils down to

$$g_2(ah^*(a, b))x_z = x_+$$

which can be recast into

$$g_2(ah^*(a, b))\sqrt{\frac{1 + ah^*(a, b)}{ah^*(a, b)}} = 1.$$

Let $\tilde{z} = ah^*(a, b)$ be a solution of such equation. Since $\tilde{z}$ is a constant independent of a and b, we then have

$$h^*(a, b) = \frac{1}{a}\tilde{z} = \frac{1}{a}h^*(1, 1).$$

References

1. Chua, L.O.: Memristor-the missing circuit element. IEEE Trans. Circuit Theory **18**(5), 507–519 (1971)

2. Corinto, F., Forti, M., Chua, L.O.: Nonlinear Circuits and Systems with Memristors. Springer, Switzerland (2021)
3. Corinto, F., Di Marco, M., Forti, M., Chua, L.: Nonlinear networks with mem-elements: complex dynamics via flux-charge analysis method. IEEE Trans. Cybern. **50**(11), 4758–4771 (2020)
4. Corinto, F., Forti, M.: Complex dynamics in arrays of memristor oscillators via the flux–charge method. IEEE Trans. Circuits Syst. I Reg. Papers **65**(3), 1040–1050 (2017)
5. Lai, Q., Wan, Z., Zhang, H., Chen, G.: Design and analysis of multiscroll memristive Hopfield neural network with adjustable memductance and application to image encryption. IEEE Trans. Neural Netw. Learn. Syst. (2022). https://doi.org/10.1109/TNNLS.2022.3146570
6. Itoh, M., Chua, L.O.: Memristor oscillators. Int. J. Bifurc. Chaos **18**(11), 3183–3206 (2008)
7. Ascoli, A., Demirkol, A.S., Tetzlaff, R., Chua, L.O.: Edge of chaos explains Prigogine's instability of the homogeneous. IEEE J. Emerg. Select. Top. Circuits Syst. **12**(4), 804–820 (2022)
8. Buscarino, A., Fortuna, L., Frasca, M., Gambuzza, L.V.: A gallery of chaotic oscillators based on HP memristor. Int. J. Bifurc. Chaos **23**(05), 1330015 (2013)
9. Liang, Y., Wang, G., Chen, G., Dong, Y., Yu, D., Iu, H.H.-C.: S-Type locally active memristor-based periodic and chaotic oscillators. IEEE Trans. Circuits Syst. I Regul. Papers **67**(12), 5139–5152 (2020)
10. Ascoli, A., Demirkol, A.S., Tetzlaff, R., Chua, L.O.: Edge of chaos theory resolves Smale paradox. IEEE Trans. Circuits Syst. I Regul. Papers **69**(3), 1252–1265 (2022)
11. Li, Y., Wang, M., Chang, H., Wang, H., Chen, G.: A hyperchaotic memristive system with extreme multistability and conservativeness. Nonlinear Dyn. **112**, 3851–3868 (2024)
12. Kumar, S., Strachan, J.P., Williams, R.S.: Chaotic dynamics in nanoscale NbO_2 Mott memristors for analogue computing. Nature **548**(7667), 318 (2017)
13. Pappachen James, A., Nabil Salama, K., Li, H., Biolek, D., Indiveri, G., Chua, L.O.: Guest editorial: Special issue on large-scale memristive systems and neurochips for computational intelligence. IEEE Trans. Emerg. Top. Comput. Intell. **2**(5), 320–323 (2018)
14. Sirakoulis, G.C., Ascoli, A., Tetzlaff, R., Yu, S.: Guest editorial: memristive circuits and systems for edge-computing applications. IEEE J. Emerg. Sel. Top. Circuits Syst. **12**(4), 717–722 (2022)
15. Stanley Williams, R.: What's next? [The end of Moore's law]. Comput. Sci. Eng. **19**(2), 7–13 (2017)
16. Ielmini, D., Philip Wong, H.-S.: In-memory computing with resistive switching devices. Nat. Electron. **1**(6), 333–343 (2018)
17. Sebastian, A., Le Gallo, M., Burr, G.W., Kim, S., Brightsky, M., Eleftheriou, E.: Tutorial: brain-inspired computing using phase-change memory devices. J. Appl. Phys. **124**(11), 111101 (2018)
18. Huang, T., Chen, Y., Zeng, Z., Chua, L.O.: Editorial special issue for 50th birthday of memristor theory and application of neuromorphic computing based on memristor-part I. IEEE Trans. Circuits Syst. I: Reg. Papers **68**(11), 4417–4418 (2021)
19. Xu, B., Zou, S., Bai, L., Chen, K., Zhao, J.: A general discrete memristor emulator based on Taylor expansion for the reconfigurable FPGA implementation and its application. Nonlinear Dyn. **112**(2), 1395–1414 (2024)
20. Itoh, M., Chua, L.O.: Memristor Cellular Automata and Memristor Discrete-Time Cellular Neural Networks, pp. 649–713. Springer International Publishing, Cham (2014)
21. Solan, E., Ochs, K.: Wave digital emulation of general memristors. Int. J. Circuit Theory Appl. **46**(11), 2011–2027 (2018)
22. Balatti, S., Ambrogio, S., Carboni, R., Milo, V., Wang, Z., Calderoni, A., Ramaswamy, N., Ielmini, D.: Physical unbiased generation of random numbers with coupled resistive switching devices. IEEE Trans. Electron Devices **63**(5), 2029–2035 (2016)
23. Li, H., Hua, Z., Bao, H., Zhu, L., Chen, M., Bao, B.: Two-dimensional memristive hyperchaotic maps and application in secure communication. IEEE Trans. Ind. Electron. **68**(10), 9931–9940 (2020)
24. Deng, Y., Li, Y.: A 2D hyperchaotic discrete memristive map and application in reservoir computing. IEEE Trans. Circuits Syst. II Express Briefs **69**(3), 1817–1821 (2021)
25. Lin, H., Wang, C., Cui, L., Sun, Y., Xu, C., Yu, F.: Brain-like initial-boosted hyperchaos and application in biomedical image encryption. IEEE Trans. Ind. Inform. **18**(12), 8839–8850 (2022)
26. Zhang, S., Zhang, H., Wang, C.: Dynamical analysis and applications of a novel 2-D hybrid dual-memristor hyperchaotic map with complexity enhancement. Nonlinear Dyn. **111**(16), 15487–15513 (2023)
27. Peng, Y., Sun, K., He, S.: A discrete memristor model and its application in Hénon map. Chaos Solitons Fractals **137**, 109873 (2020)
28. Bao, H., Hua, Z., Li, H., Chen, M., Bao, B.: Discrete memristor hyperchaotic maps. IEEE Trans. Circuits Syst. I Reg. Papers **68**(11), 4534–4544 (2021)
29. Bao, H., Gu, Y., Xu, Q., Zhang, X., Bao, B.: Parallel bi-memristor hyperchaotic map with extreme multistability. Chaos Solitons Fractals **160**, 112273 (2022)
30. Bao, H., Li, H., Hua, Z., Xu, Q., Bao, B.: Sine-transform-based memristive hyperchaotic model with hardware implementation. IEEE Trans. Ind. Inf. **19**(3), 2792–2801 (2022)
31. Ma, M., Yang, Y., Qiu, Z., Peng, Y., Sun, Y., Li, Z., Wang, M.: A locally active discrete memristor model and its application in a hyperchaotic map. Nonlinear Dyn. **107**(3), 2935–2949 (2022)
32. Lai, Q., Yang, L., Chen, G.: Design and performance analysis of discrete memristive hyperchaotic systems with stuffed cube attractors and ultraboosting behaviors. IEEE Trans. Ind. Electron. (2023). https://doi.org/10.1109/TIE.2023.3299016
33. Deng, Y., Li, Y.: Nonparametric bifurcation mechanism in 2-D hyperchaotic discrete memristor-based map. Nonlinear Dyn. **104**(4), 4601–4614 (2021)
34. Bao, B.C., Bao, H., Wang, N., Chen, M., Xu, Q.: Hidden extreme multistability in memristive hyperchaotic system. Chaos Solitons Fractals **94**, 102–111 (2017)
35. Lai, Q., Wan, Z., Kengne, L.K., Kamdem Kuate, P.D., Chen, C.: Two-memristor-based chaotic system with infinite coexisting attractors. IEEE Trans. Circuits Syst. II: Express Briefs **68**(6), 2197–2201 (2020)
36. Lai, Q., Lai, C., Zhang, H., Li, C.: Hidden coexisting hyperchaos of new memristive neuron model and its application

in image encryption. Chaos Solitons Fractals **158**, 112017 (2022)

37. Corinto, F., Forti, M.: Memristor circuits: flux-charge analysis method. IEEE Trans. Circuits Syst. I: Regul. Papers **63**(11), 1997–2009 (2016)

38. Corinto, F., Forti, M.: Memristor circuits: bifurcations without parameters. IEEE Trans. Circuits Syst. I Regul. Papers **64**(6), 1540–1551 (2017)

39. Di Marco, M., Forti, M., Pancioni, L., Tesi, A.: New class of discrete-time memristor circuits: first integrals, coexisting attractors and bifurcations without parameters. Int. J. Bifurc. Chaos **34**(01), 2450001 (2024)

40. Li, T.-Y., Yorke, J.A.: Period three implies chaos. Am. Math. Mon. **82**(10), 985–992 (1975)

41. Marotto, F.R.: Snap-back repellers imply chaos in R^n. J. Math. Anal. Appl. **63**(1), 199–223 (1978)

42. Li, C., Chen, G.: An improved version of the Marotto theorem. Chaos Solitons Fractals **18**(1), 69–77 (2003)

43. Hale, J., Koçak, H.: Dynamics and Bifurcations. Springer-Verlag, New York (1991)